



Quantifying the passive stretching response of human tibialis anterior muscle using shear wave elastography

Terry K. Koo^{a,*}, Jing-Yi Guo^a, Jeffrey H. Cohen^b, Kevin J. Parker^c

^a Department of Research, New York Chiropractic College, Seneca Falls, NY, United States

^b Nimmo® Educational Foundation, Pittsburgh, PA, United States

^c Dept. of Electrical & Computer Engineering, University of Rochester, Rochester, NY, United States

ARTICLE INFO

Article history:

Received 24 June 2013

Accepted 11 November 2013

Keywords:

Shear wave elastography

Shear elastic modulus

Tibialis anterior

Passive stretch

Muscle contracture

Anterior compartment syndrome

Reliability

ABSTRACT

Background: Quantifying passive stretching responses of individual muscles helps the diagnosis of muscle disorders and aids the evaluation of surgical/rehabilitation treatments. Utilizing an animal model, we demonstrated that shear elastic modulus measured by supersonic shear wave elastography increases linearly with passive muscle force. This study aimed to use this state-of-the-art technology to study the relationship between shear elastic modulus and ankle dorsi–plantarflexion angle of resting tibialis anterior muscles and extract physiologically meaningful parameters from the elasticity–angle curve to better quantify passive stretching responses.

Methods: Elasticity measurements were made at resting tibialis anterior of 20 healthy subjects with the ankle positioned from 50° plantarflexion to up to 15° dorsiflexion at every 5° for two cycles. Elasticity–angle data was curve–fitted by optimizing slack angle, slack elasticity, and rate of increase in elasticity within a piecewise exponential model.

Findings: Elasticity–angle data of all subjects were well fitted by the piecewise exponential model with coefficients of determination ranging between 0.973 and 0.995. Mean (SD) of slack angle, slack elasticity, and rate of increase in elasticity were 10.9° (6.3°), 5.8 (1.9) kPa, and 0.0347 (0.0082) respectively. Intraclass correlation coefficients of each parameter were 0.852, 0.942, and 0.936 respectively, indicating excellent test–retest reliability.

Interpretation: This study demonstrated the feasibility of using supersonic shear wave elastography to quantify passive stretching characteristics of individual muscle and provided preliminary normative values of slack angle, slack elasticity, and rate of increase in elasticity for human tibialis anterior muscles. Future studies will investigate diagnostic values of these parameters in clinical applications.

© 2013 Elsevier Ltd. All rights reserved.

1. Introduction

The study of passive stretching response of individual muscles can help the diagnosis of muscle disorders and aids the evaluation of surgical and rehabilitation treatments. In animal studies, the characteristics of passive stretching have been evaluated by quantifying the passive tension–length relationships at both single fiber (Gordon et al., 1966) and whole muscle level (Winters et al., 2011). However, in human studies, since direct, non-invasive measurement of passive muscle force is still beyond the current state-of-the-art, passive torque–angle measurements have been widely used instead (Gajdosik et al., 2005; McNair et al., 2002; Weiss et al., 1986). The limitations of torque–angle measurements are that rather than a single muscle, they only reflect

the resultant of many structures crossing the joint. These measurements are further compromised by the differences in moment arms among various structures. Hence passive torque–angle measurements are non-specific measures of the passive stretching responses of individual muscles.

More recently, optimization methods have been used to estimate the passive tension–length relationship in vivo but these methods are only applicable to two-joint muscles such as gastrocnemius (Hoang et al., 2005; Nordez et al., 2010). In these methods, passive torque–angle data of the ankle joint were used to estimate the parameters of the gastrocnemius tension–length curves based on the assumptions that: (1) changes in torque–angle curves of the ankle joint at different knee angles are due to changes in the length of the gastrocnemius only; (2) passive tension in the gastrocnemius is an exponential function of the gastrocnemius length; and (3) moment arms of the gastrocnemius muscle can be reasonably estimated from cadaveric data (Grieve et al., 1978). Violation of any of these assumptions will affect the validity of the passive tension–length predication. Therefore,

* Corresponding author at: Foot Levelers Biomechanics Research Laboratory, New York Chiropractic College, 2360 State Route 89, Seneca Falls, NY 13148, United States.

E-mail address: tkoo@nycc.edu (T.K. Koo).

a non-invasive technique that could provide indirect measurement of passive muscle force would be valuable for human studies.

Baumann et al. (1979) proposed that intramuscular pressure (i.e. the hydrostatic fluid pressure within a muscle) may provide an estimate of passive muscle force. However, direct measurements of intramuscular pressure and passive muscle force in isolated rabbit tibialis anterior muscle only revealed a modest correlation with wide variation between specimens (Davis et al., 2003), indicating that intramuscular pressure may not be a reliable indirect measure of passive muscle force.

Recently, a state-of-the-art ultrasound technology, namely supersonic shear wave elastography (SSWE), has been developed that allows for non-invasive and reliable measurement of muscle elasticity (Bercoff et al., 2004a; Koo et al., 2013; Lacourpaille et al., 2012). Briefly speaking, SSWE uses acoustic radiation force induced by ultrasound beams to perturb muscle tissues. This force induces shear waves which propagate within the muscle. By focusing the push forces at different depths within the muscle at high speed, shear waves are coherently summed, which substantially increase the propagation distance, yet minimize the acoustic power to the muscle (Bercoff et al., 2004b). As the shear waves propagate, they are captured by the ultrasound transducer at an ultrafast frame rate. Shear wave propagation speed (V) is then estimated at each pixel using cross-correlation algorithm. Shear elastic modulus (G) can then be calculated by the following equation (Bercoff et al., 2004a):

$$G = \rho V^2 \quad (1)$$

where ρ is the muscle density which is assumed to be 1000 kg/m³.

Maisetti et al. (2012) conducted a human experiment on gastrocnemius muscle and provided the first evidence to support the use of SSWE for indirect estimation of passive muscle force. In an ex vivo study of 32 chicken muscles, we further confirmed that there was a strong linear relationship (mean $R^2 = 0.9875$; range: 0.9741 and 0.9943) between passive muscle tension (induced by calibrated weights) and shear elastic modulus (measured by SSWE) (Koo et al., 2013), and hence, SSWE elasticity measurements can be regarded as an indirect measure of passive muscle force. Therefore, when SSWE elasticity of a resting single joint muscle is plotted against joint angles, the elasticity–angle curve can reflect muscle-specific passive stretching response of the tested muscle.

Objectives of the present study were to extend our recent work to healthy human subjects to: (1) determine the test–retest reliability of SSWE for in vivo measurements of passive muscle elasticity of the tibialis anterior (TA) muscle; (2) evaluate the relationship between SSWE elasticity and ankle dorsi–plantarflexion angle of the TA muscle; and (3) extract physiologically meaningful parameters from the elasticity–angle curves for better quantification of passive stretching response. Since compartment syndrome most often occurs in the anterior compartment of the lower leg, selection of the TA as our targeted muscle would not only allow us to evaluate the passive stretching response of the TA muscle, but also may provide insights to guide our future research directions of using SSWE towards non-invasive diagnosis and/or prognosis of anterior compartment syndrome.

2. Methods

2.1. Subjects

Convenient samples of 20 healthy subjects (11 women and 9 men) were recruited from the student and staff population of New York Chiropractic College (NYCC). Subjects gave informed consent to the investigation according to the procedure approved by the institutional review board of NYCC. Mean (SD) of age, height, and weight of the male and female groups were 28.7 (8.8) years, 176.9 (7.3) cm, 74.4 (6.6) kg, and 33.2 (14.9) years, 163.8 (4.6) cm, 58.6 (6.2) kg respectively.

2.2. Ankle angle measurements

Special care was taken to define the neutral position of the ankle joint using an electrogoniometer (Biometrics, Newport, UK). The electrogoniometer was adhered to the medial aspect of the ankle joint. Subjects were instructed to face forward and stand upright with their feet separated to align with their shoulders. The neutral position (i.e. 0°) was then registered by zeroing the electrogoniometer at this pose. Once the neutral position was defined, subjects were instructed to sit comfortably on an assessment chair of a dynamometer system (Biodex Medical Systems, Shirley, NY) with their left foot placed on a footplate that anchored to the dynamometer (Fig. 1). The footplate settings were adjusted until the dorsi/plantarflexion axis of the ankle joint aligned with the axis of rotation of the dynamometer. The assessment chair position was further adjusted so that the plantar surface of the foot did not push against the footplate when the ankle joint was passively rotated throughout the testing range (i.e. 50° plantarflexion to 15° dorsiflexion). It was noted that these arrangements could minimize shank movement as the ankle was being rotated. In addition, the knee was fixed at ~30° flexion to avoid overstretching of the gastrocnemius muscle at dorsiflexed positions. A custom-made stabilizer was fixed around the knee to support the leg and constraint it from mediolateral displacement (Fig. 1). After subjects were properly positioned, angle reading from the dynamometer was set to zero when the ankle joint was positioned at the neutral position as defined by the electrogoniometer. All ankle joint positioning afterwards was based on the readings from the dynamometer.

2.3. Shear elastic modulus measurements

An Aixplorer ultrasound scanner (Supersonic Imagine, Aix en Provence, France), coupled with a 50 mm long SL-15-4 linear ultrasound transducer was set to the SSWE mode to measure shear elastic modulus of the left tibialis anterior (TA) muscles. The SSWE mode composes of three steps: pushing, imaging, and processing. First, a series of ultrasound “push” beams (center frequency = 6.0 MHz) were focused at different depths of the muscle, creating two intense plane shear waves. After the creation of the plane shear waves, the system immediately switched to “imaging” mode and used the same transducer (center frequency = 7.5 MHz) to detect propagation of the shear waves at a frame rate of up to 20,000 Hz. Lastly, shear wave propagation speeds were calculated at each pixel using one-dimensional cross-correlation algorithm. A mounting apparatus that consisted of an articulated arm, a linear actuator, and a mounting jig was developed to position and hold the ultrasound transducer at desired locations (Fig. 1). Briefly speaking, the articulated arm (Manfrotto, Italy) possessed multiple degrees of freedom joints and a center lock to facilitate precise positioning and quick locking of the ultrasound transducer. The linear actuator (Zaber Technologies, Vancouver, Canada) allowed for precise positioning of the transducer so as to minimize tissue compression throughout the elasticity measurements. It has been shown that soft tissue could become artificially stiffer under compression (Gennisson et al., 2007; Slapa et al., 2012).

The ultrasound transducer was positioned on the muscle belly of the left TA along its longitudinal axis at proximal one-third level of the leg (Fig. 1). Appropriate transducer alignment was confirmed by tracing several fascicles without interruption across the B-mode image (Blazevich et al., 2006). Transducer orientation was further adjusted until the central aponeurosis of the TA could be clearly seen (Fig. 2). Once the B-mode image was optimized and the articulated arm was locked, the linear actuator was retracted to create a small gap between the transducer and skin surface (Fig. 2). Generous amount of ultrasound gel was then applied to fill the gap.

For each TA muscle, a rectangular-shape elastography window (23 mm × 17 mm) was positioned right below the upper boundary of

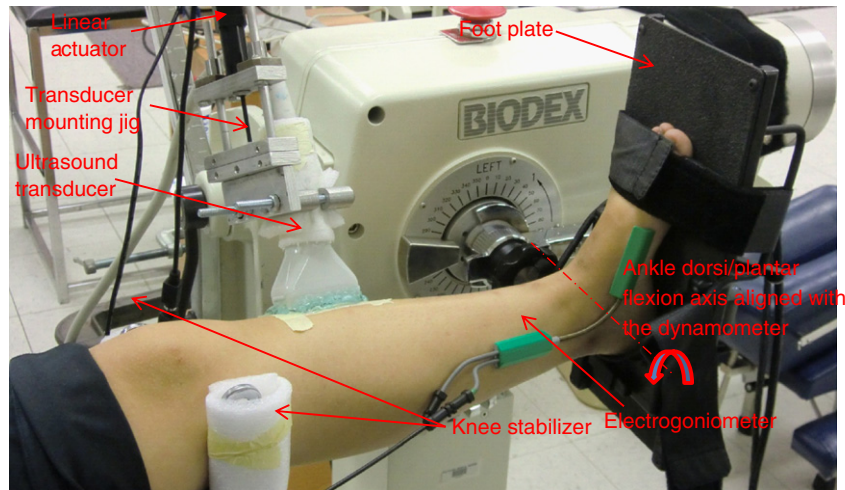


Fig. 1. Experimental setup. A mounting apparatus that consists of an articulated arm, a linear actuator, and a mounting jig was developed to position and hold the ultrasound transducer at desired locations. The articulated arm was not shown. A custom-made stabilizer was fixed around the knee to support the leg and constraint it from mediolateral displacement.

the TA muscle (Fig. 2). A circular region between the upper boundary and the central aponeurosis of the TA muscle was selected in the middle of the elastography window to facilitate direct comparison of the elasticity data between different ankle angles and cycles.

2.4. Experimental protocol

SSWE elasticity measurements were made with the ankle joint positioned from 50° plantarflexion (i.e. 50°) to up to 15° dorsiflexion (i.e. –15°) at every 5° for two cycles. At each angle, the elastography window was first allowed to stabilize for 5 s before the 1st elastography image was acquired. The 2nd and 3rd elastography

images were then captured 3 and 6 s later (Koo et al., 2013). For each image, average shear elastic modulus within the circular region was calculated and the ensemble mean among the 3 images was regarded as the shear elastic modulus of the tested muscle at that angle. Coefficients of variation (CV) of the shear elastic modulus among the 3 images were calculated at each angle to assess the quality of our measurements. In addition, validity of each elasticity measurement was confirmed by reviewing the quality of the corresponding shear wave propagation movie (Koo et al., 2013). Briefly speaking, shear wave propagation movie is a special tool within the research software provided by the manufacturer. It allows for direct visualization of the propagation of the shear waves induced by

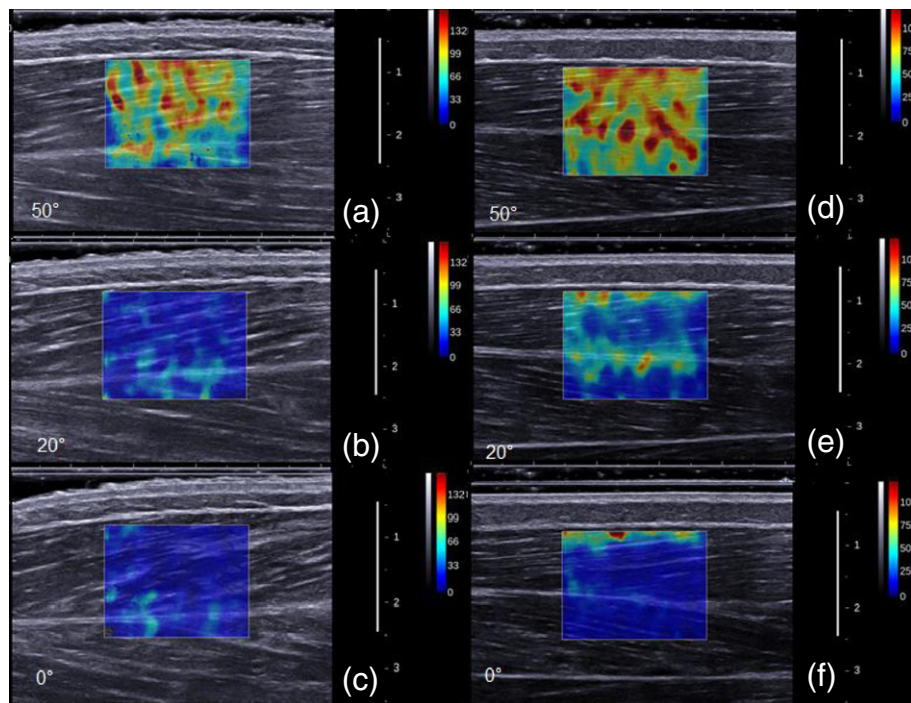


Fig. 2. Examples of elastography images of tibialis anterior. Two elastography patterns observed in the tested subjects. Pattern I (left column): at 50°; at 20°; and at 0°. Pattern II (right column): at 50°; at 20°; and at 0°. For Pattern I, elastography map was rather uniform between the superficial and deep TA fibers at each angle. For Pattern II, although the shear elastic modulus of the deeper muscle fibers decreased concomitantly with dorsiflexion as expected, the superficial layer was getting stiffer as the plantarflexion angle decreased. To minimize compression artifact, a small gap was maintained between transducer and skin surface for all measurements. Similar muscle fascicle patterns were noted in B-mode ultrasound images at different ankle angles, indicating the same transducer orientation was maintained throughout the measurements. An image sequence of a representative subject is included as Supplementary online material to further demonstrate the quality of our measurements (Appendix A). Color scale represents shear elastic modulus in kilopascal. Images from each column are shown at the same scale.

acoustic radiation forces. Ideally, the acoustic radiation forces induce a pair of strong plane shear waves that propagate in opposite directions (cf. Fig. 2a of Koo et al., 2013). The stiffer the medium, the faster the shear wave will move. With strong shear waves, the shear wave propagation speed can be reliably estimated at each pixel from the shear wave propagation movie using cross correlation algorithms. Conversely, if the induced shear waves are weak, as they propagate, dissipation will occur rapidly and hence, shear wave signals will disperse quickly (cf. Fig. 2b of Koo et al., 2013), making the shear wave propagation speed estimation unreliable. Therefore, by observing the integrity of the shear wave propagation, we can assess the quality of our elasticity measurements.

Throughout the experiment, subjects were instructed to relax completely and avoid any movement distal to the hips. During elasticity measurements, an investigator continuously monitored the real time B-mode ultrasound images to make sure that there was no subtle movement at the shank or unconscious contraction of the TA muscle.

2.5. Parameter extraction

To extract physiologically meaningful parameters from the elasticity–angle data, a piecewise exponential model that has been widely used to describe the passive tension–length relationship of skeletal muscle (Giat et al., 1994; Hoang et al., 2005; Koo et al., 2002; Zajac, 1989) was modified to curve-fit the data:

$$\begin{aligned} G(\theta) &= G_o && \text{if } \theta \leq \theta_o \\ G(\theta) &= G_o \left(e^{\alpha(\theta - \theta_o)} \right) && \text{if } \theta > \theta_o \end{aligned} \quad (2)$$

where $G(\theta)$ is the shear elastic modulus of a resting TA muscle at angle θ ; θ_o is the slack angle – the ankle angle at which the TA becomes slack; G_o is the slack elasticity – the shear elastic modulus of the TA when it becomes slack; and α is related to the rate of elasticity build up as the TA is being stretched.

A Matlab program (MathWorks, Natick, MA) was developed to optimize $[\theta_o, G_o, \alpha]$ by minimizing the square difference between the experimentally measured and modeled shear elastic modulus using Levenberg–Marquardt algorithm. Coefficient of determination (R^2) of each fit was calculated. Net increased in shear elastic modulus at 50° plantarflexion (i.e. $\Delta G_{50} = G(50^\circ) - G_o$) was also calculated to quantify the overall stretch response after the TA muscle became taut.

2.6. Statistical analysis

Test–retest reliability of each parameter (i.e. $\theta_o, G_o, \alpha, \Delta G_{50}$) was calculated based on a single-rating, absolute-agreement, 2-way mixed effect model (intraclass correlation coefficient $ICC_{3,1}$) (McGraw and Wong, 1996). Effect of gender on each variable was evaluated using independent t-tests. Post hoc power analysis was used to compute the achieved power of the independent t-tests. All statistical analyses were conducted using SPSS statistical package version 19 (SPSS, Chicago, IL) except for the post hoc power analysis, which was performed by G*Power 3 (Faul et al., 2007). A confidence level of 0.05 was chosen for all statistical tests.

3. Results

A careful evaluation of SSWE images revealed two distinct elastography patterns. Fig. 2 (left) shows SSWE images of a TA muscle at 50°, 20°, and 0° with Pattern I; and Fig. 2 (right) shows corresponding SSWE images of a TA muscle with Pattern II. Generally speaking, the elastography windows were rather uniform between the superficial and deep TA fibers in 10 subjects (7 women, 3 men) (Pattern I). In another 10 subjects (4 women, 6 men), although the shear elastic modulus of the deeper muscle fibers decreased

concomitantly with dorsiflexion as expected, the superficial layer was getting stiffer as the plantarflexion angle decreased (Pattern II). We believed that Pattern II is related to the compressive effect of crural fascia against the superficial TA layer. More interpretations will be covered in the “Discussions” section. Nonetheless, the elasticity measurements at the superficial TA layer of Pattern II could be considered as compression artifact, and hence, they were avoided when selecting the circular region for elasticity measurements. To test whether the compressive effect of crural fascia would also stiffen up the deep TA layer, subjects were grouped and compared based on their SSWE image patterns. It revealed that all parameters were not significantly different between patterns ($\theta_o: P = 0.167$; $G_o: P = 0.199$; $\alpha: P = 0.893$; $\Delta G_{50}: P = 0.927$), indicating that the compressive effect of crural fascia on the shear elastic modulus of the deep TA layer is minimal.

Mean (SD) of coefficients of variation (CV) of the shear elastic modulus measurements among subjects is 1.92 (1.63)%, indicating excellent repeatability of the SSWE measurements. CVs of individual subjects are summarized in Table 1. Fig. 3 shows a representative elasticity–angle plot of the TA muscle for two consecutive cycles. Generally speaking, the two cycles were very similar. The shear elastic modulus was relatively constant in the beginning and started to pick up its nonlinearity after the ankle getting beyond the slack angle (i.e. $\theta_o = 10.6^\circ$). Test–retest reliability of the elasticity–angle relationship was very good for θ_o ($ICC = 0.852$) and excellent for G_o ($ICC = 0.942$); α ($ICC = 0.936$); and ΔG_{50} ($ICC = 0.970$) respectively. In addition, the elasticity–angle relationships of all subjects were well fitted by the piecewise exponential model with mean (SD) coefficient of determination (R^2) equaled 0.985 (0.0064) and ranged between 0.973 and 0.995.

Mean (SD) of θ_o, α, G_o and ΔG_{50} of the male and female subject groups are shown in Fig. 4. It revealed that all parameters were not significantly different between gender groups ($\theta_o: P = 0.870$; $G_o: P = 0.072$; $\alpha: P = 0.171$; $\Delta G_{50}: P = 0.331$). Their pooled mean (SD) were $\theta_o = 10.9^\circ$ (6.3°), $G_o = 5.8$ (1.9) kPa, $\alpha = 0.0347$ (0.0082), and $\Delta G_{50} = 17.2$ (6.5) kPa.

4. Discussions

The present study shows that with proper setup, SSWE can be used to make reliable in vivo measurements of passive TA elasticity. The high reproducibility of our measurements can be attributed to our success of: (1) maintaining the transducer orientation and location throughout the

Table 1
Coefficients of variation (CV) of the shear elastic modulus.

Subject	Coefficients of variation ^a (%)	
	Mean	SD
1	1.95	1.16
2	0.95	0.50
3	1.39	0.91
4	1.73	1.04
5	1.76	1.16
6	0.82	0.66
7	1.91	1.30
8	1.80	1.80
9	3.26	3.15
10	1.85	1.32
11	2.01	1.04
12	1.94	2.00
13	1.20	1.59
14	1.33	0.77
15	2.57	1.58
16	1.48	0.93
17	2.11	1.97
18	1.68	1.36
19	3.02	2.48
20	2.37	1.63

^a CVs at each tested angle were averaged and reported as mean (SD) for each subject.

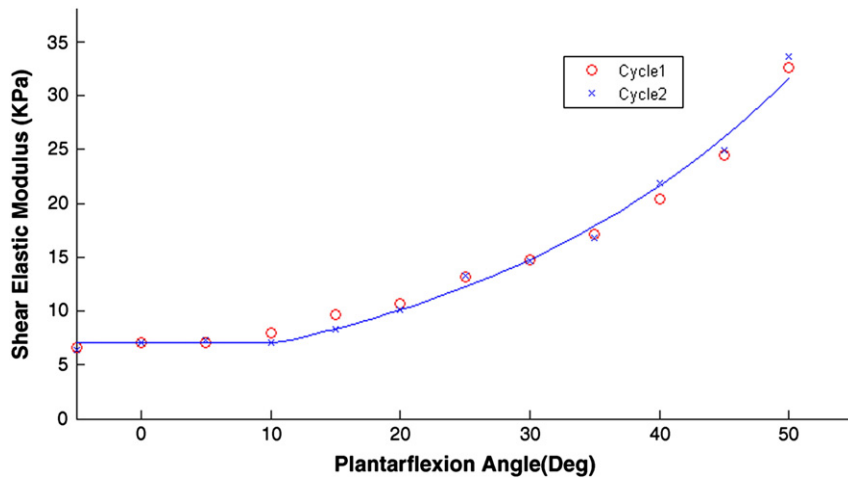


Fig. 3. Representative example of the passive elasticity–angle plot of two consecutive cycles showing the repeatability of the measurements. A piecewise exponential model was fitted to the data and superimposed to the same graph to show the goodness of fit ($R^2 = 0.9906$). For this subject, $\theta_0 = 10.6^\circ$, $\alpha = 0.038$; $G_0 = 7.1$ kPa; and $\Delta G_{50} = 26.0$ kPa.

measurements using a mounting apparatus; (2) minimizing tissue compression by adjusting the transducer height using a linear actuator; and (3) validating the SSWE images using shear wave movies. To the author’s knowledge, there was only one study in the literature explicitly reported the use of shear wave propagation movies as a quality control of the SSWE data (Koo et al., 2013).

Apart from the TA muscle, we anticipate that other muscles with good shear wave signals can also be reliably measured. For instance, we collected preliminary SSWE data of the upper trapezius, erector

spinae across the lumbar region, lumbar multifidus, biceps brachii, and brachioradialis, and observed the quality of their shear wave propagation movies. It revealed that shear waves were poorly generated and propagated within the upper trapezius, lumbar erector spinae, and lumbar multifidus, and hence, the SSWE data collected at these muscles must be interpreted with caution. Conversely, shear wave propagation movies of the biceps brachii and brachioradialis muscles were good, indicating that SSWE could be used to make reliable measurements on these muscles. The exact reasons why some muscles work better than the other are not well understood. One possible explanation may be related to the attenuation effect of skin and subcutaneous tissues. Although not systematically evaluated in this study, we noted that muscles covered by thick layers of skin and subcutaneous tissues appeared to have poorer shear wave signals and the penetration depth of the acoustic radiation force also appeared to be lesser. Nonetheless, a separate study is needed to confirm this observation.

Estimating muscle lengths from musculoskeletal models involves many empirical assumptions about muscle paths and musculotendon parameters, which makes the estimation doubtful. On the other hand, direct measurements of muscle fascicle lengths can be a subjective task because muscle fascicle lengths depend on transducer placement and they can vary widely within the same muscle (Diong et al., 2012; Kwah et al., 2012). Instead of utilizing musculoskeletal models or ultrasound imaging to estimate/measure muscle lengths and plotting against muscle elasticity, we opted to report the elasticity–angle relationship, mainly because joint angles can be directly measured in an accurate manner. Another advantage of reporting the elasticity–angle relationship is that it puts muscle function into context because muscle acts across joint to generate motion.

We successfully curve-fitted the passive elasticity–angle data using a piecewise-exponential model with three parameters (θ_0 , G_0 , α). Since such a model has been shown to fit passive tension–length relationship of skeletal muscle well (Zajac, 1989), our results appear to further support the idea that SSWE can provide indirect measurements of passive muscle force (Koo et al., 2013; Maisetti et al., 2012).

By definition, optimal muscle fiber length is the length where passive muscle force comes into play and active force component maximizes (Koo et al., 2002; Zajac, 1989). For a single joint muscle like TA, the corresponding ankle angle at which the muscle fiber length equals the optimal muscle fiber length is defined as muscle optimal angle (Koo et al., 2002). If passive muscle force is linearly related to SSWE shear elastic modulus, this muscle optimal angle is equivalent to the slack angle (θ_0) identified in this study. Based on muscle architectural parameters of the tibialis anterior muscle measured from 21 cadavers (Ward et al., 2009), Arnold and Delp (2011)

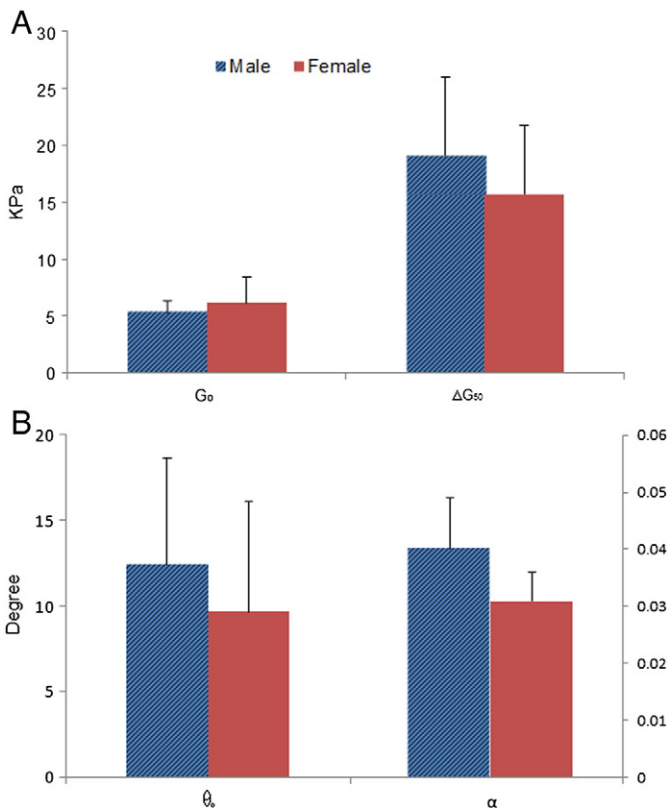


Fig. 4. Mean (SD) of θ_0 , α , G_0 , and ΔG_{50} of the male and female subject groups. θ_0 : the ankle angle at which the TA becomes slack; G_0 : the shear elastic modulus of the TA when it becomes slack; ΔG_{50} : net increased in shear elastic modulus at 50° plantarflexion (i.e. $\Delta G_{50} = G(50^\circ) - G_0$). No significant difference between gender groups was found for all parameters. Error bar stands for 1 SD.

simulated the TA muscle fiber lengths across percentage of gait cycle and found that the optimal angle of the TA muscle is about 12° (cf. Figs. 3 & 6 of Arnold and Delp, 2011), which agrees well with our θ_0 measurements (mean $\theta_0 = 10.9^\circ$). This agreement further supports the validity of our measurements. In clinical practice, θ_0 may be used to quantify muscle contracture resulting from immobilization, spasticity, and muscle weakness. Effects of different treatments such as passive stretching, splinting, electrical stimulation, tendon transfer, and tendon lengthening surgery may also be evaluated by comparing θ_0 before and after a treatment. Similarly, treatment effect may also be quantified by the change in ΔG_{50} pre- and post-intervention.

G_0 represents the shear elastic modulus of a relaxed muscle at its slack length. Our measurements (mean = 5.8 kPa) were comparable with those reported by Lacourpaille et al. (2012) (mean = 4.5 kPa). It appears that the slight difference can be attributed to the difference in measurement protocols between the two studies. Lacourpaille measured shear elastic modulus of the TA muscle with the ankle in the neutral position (i.e. 0°) but our study was based on curve-fitting the passive elasticity–angle data from 50° plantarflexion to up to 15° dorsiflexion. Koo et al. (2013) reported that G_0 does not correlate with muscle cross sectional area. Instead, it appears to be related to the amount and type of collagen fibers within a muscle (Kovanen et al., 1984). Hence, G_0 could be a useful parameter for the diagnosis of connective tissue related pathologies. It may also be related to the muscle tone of a resting muscle. The third parameter, α , is related to the rate of elasticity build up as a muscle is being stretched. If a within-subjects comparison of α is made before and after an intervention, this parameter could reflect the change in muscle stiffness. However, α could be affected by joint geometry, muscle slack length, muscle cross sectional area, mechanical properties of a muscle, etc., and hence, it may be difficult to interpret for between-subjects comparison.

Since TA muscle length reduces with dorsiflexion, we would expect a gradual decrease in shear elastic modulus of the whole TA muscle as the ankle joint is being dorsiflexed. Surprisingly, this pattern only showed up in 50% of the subjects (Fig. 2a–c). For another 50% of the tested subjects, although the shear elastic modulus of the deeper fascicles decreased concomitantly with dorsiflexion, the shear elastic modulus of the superficial TA layer increased with dorsiflexion (Fig. 2d–f). When a non-constrained muscle is passively shortened, its thickness increases. However, that is not the case for an in-situ TA muscle. Due to the fact that there is a tight and dense layer of anterior crural fascia covered the TA muscle in situ, it limits the TA muscle from increasing thickness. Instead, the crural fascia may compress against the superficial layer of the TA muscle. Depending on the tightness of the crural fascia, the muscle size, and the amount of thickness change during dorsiflexion, the compression can become large enough to artificially stiffen the superficial layer of the TA muscle. That may explain why some subjects showed substantial increased in shear elastic modulus at the superficial layer of the TA muscle as the ankle was getting close to the neutral position but some were not. It appears that this compression artifact may predispose athletes who participate in sports that involve repetitive loading or exertional activities to a higher risk of developing anterior chronic exertional compartment syndrome. Nonetheless, a longitudinal study needs to be done to test this hypothesis. It could be achieved by comparing the proportion of subjects showed Pattern showing Patterns I and II that actually develop the syndrome. Currently, direct measurement of intramuscular pressure by insertion of a catheter into the muscle at risk is a gold standard for clinical diagnosis of compartment syndrome (Lynch et al., 2009). SSWE may be a non-invasive alternative to clinical diagnosis of compartment syndrome (Lv et al., 2012).

The present work was not without limitations. First, even though there was no relative movement between the transducer and skin surface, and the elastography window was fixed at the same location of all SSWE images, we still could not measure the exact same region of

the TA muscle at different ankle positions. It is because as the ankle plantarflexion angle decreases, the TA muscle fibers indeed slide slightly towards its origin (Appendix A). Nonetheless, its effect should be minimal because muscle fibers are continuum materials, and hence, their tension supposed to be homogenous along the whole fibers. Second, due to the exploratory nature of the present study, we only tested a relatively small number of male and female subjects. Post hoc power analysis revealed that the achieved powers of α , θ_0 , G_0 , and ΔG_{50} were 0.81, 0.15, 0.17, and 0.20 respectively, which were all below 0.9. Hence, the insignificant effect of gender on α , θ_0 , G_0 , and ΔG_{50} revealed in the present study should be interpreted with caution. A priori power analysis based on the current results revealed that at least 116 subjects per group is required to achieve a power of 0.9 for all parameters. Future studies should increase the sample size so that normative data of each parameter for both male and female can be established for clinical reference. Third, we did not explicitly measure muscle density but assumed that all tested muscles had a density of 1000 kg/m^3 . Indeed, the actual density of each tested muscle might be different from 1000 kg/m^3 , which could slightly affect the muscle shear modulus calculation. Nonetheless, the assumed muscle density value adopted in this study has been widely used in the literature (e.g. Eby et al., 2013; Lacourpaille et al., 2012; Maisetti et al., 2012).

In summary, we applied SSWE to human TA muscles and successfully extracted physiologically meaningful parameters from the elasticity–angle curves for better quantification of passive stretching response. Future studies should investigate the diagnostic values of each of these parameters for various clinical applications.

Conflict of interest statement

The authors confirm that there is no conflict of interest in this manuscript.

Acknowledgments

This study was partially supported by Nimmo® Educational Foundation.

Appendix A. Supplementary data

Supplementary data to this article can be found online at <http://dx.doi.org/10.1016/j.clinbiomech.2013.11.009>.

References

- Arnold, E.M., Delp, S.L., 2011. Fibre operating lengths of human lower limb muscles during walking. *Phil. Trans. R. Soc. B* 366, 1530–1539.
- Baumann, J.U., Sutherland, D.H., Hanggi, A., 1979. Intramuscular pressure during walking: an experimental study using the wick catheter technique. *Clin. Orthop. Relat. Res.* 145, 292–299.
- Bercoff, J., Tanter, M., Fink, M., 2004a. Supersonic shear imaging: a new technique for soft tissue elasticity mapping. *IEEE Trans. Ultrason. Ferroelectr. Freq. Control* 51, 396–409.
- Bercoff, J., Tanter, M., Fink, M., 2004b. Sonic boom in soft materials: the elastic Cerenkov effect. *Appl. Phys. Lett.* 84 (12), 2202–2204.
- Blazevich, A.J., Gill, N.D., Zhou, S., 2006. Intra- and intermuscular variation in human quadriceps femoris architecture assessed in vivo. *J. Anat.* 209, 289–310.
- Davis, J., Kaufman, K.R., Lieber, R.L., 2003. Correlation between active and passive isometric force and intramuscular pressure in the isolated rabbit tibialis anterior muscle. *J. Biomech.* 36, 505–512.
- Diong, J.H., et al., 2012. Passive mechanical properties of the gastrocnemius after spinal cord injury. *Muscle Nerve* 46, 237–245.
- Eby, S.F., et al., 2013. Validation of shear wave elastography in skeletal muscle. *J. Biomech.* 46, 2381–2387.
- Faul, F., et al., 2007. G*Power 3: a flexible statistical power analysis program for the social, behavioral, and biomedical sciences. *Behav. Res. Methods* 39, 175–191.
- Gajdosik, R.L., et al., 2005. Effects of an eight-week stretching program on the passive-elastic properties and function of the calf muscles of older women. *Clin. Biomech.* 20, 973–983.
- Gennisson, J.L., et al., 2007. Acoustoelasticity in soft solids: assessment of the nonlinear shear modulus with the acoustic radiation force. *J. Acoust. Soc. Am.* 122, 3211–3219.
- Ciat, Y., et al., 1994. Simulation of distal tendon transfer of the biceps brachii and the brachialis muscles. *J. Biomech.* 27, 1005–1014.

- Gordon, A.M., Huxley, A.F., Julian, F.J., 1966. The variation in isometric tension with sarcomere length in vertebrate muscle fibres. *J. Physiol.* 184, 170–192.
- Grieve, D., Pheasant, S., Cavanagh, P.R., 1978. Prediction of Gastrocnemius Length From Knee and Ankle Joint Posture.
- Hoang, P.D., et al., 2005. A new method for measuring passive length–tension properties of human gastrocnemius muscle in vivo. *J. Biomech.* 38, 1333–1341.
- Koo, T.K., Mak, A.F., Hung, L.K., 2002. In vivo determination of subject-specific musculotendon parameters: applications to the prime elbow flexors in normal and hemiparetic subjects. *Clin. Biomech.* 17, 390–399.
- Koo, T.K., et al., 2013. Relationship between shear elastic modulus and passive muscle force: an ex-vivo study. *J. Biomech.* 46, 2053–2059.
- Kovanen, V., Suominen, H., Heikkinen, E., 1984. Mechanical properties of fast and slow skeletal muscle with special reference to collagen and endurance training. *J. Biomech.* 17, 725–735.
- Kwah, L.K., et al., 2012. Passive mechanical properties of gastrocnemius muscles of people with ankle contracture after stroke. *Arch. Phys. Med. Rehabil.* 93, 1185–1190.
- Lacourpaille, L., et al., 2012. Supersonic shear imaging provides a reliable measurement of resting muscle shear elastic modulus. *Physiol. Meas.* 33, N19–N28.
- Lv, F., et al., 2012. Muscle crush injury of extremity: quantitative elastography with supersonic shear imaging. *Ultrasound Med. Biol.* 38 (5), 795–802.
- Lynch, J.E., et al., 2009. Noninvasive monitoring of elevated intramuscular pressure in a model compartment syndrome via quantitative fascial motion. *J. Orthop. Res.* 27 (4), 489–494.
- Maisetti, O., et al., 2012. Characterization of passive elastic properties of the human medial gastrocnemius muscle belly using supersonic shear imaging. *J. Biomech.* 45, 978–984.
- McGraw, K.O., Wong, S.P., 1996. Forming Inferences about some intraclass correlation coefficients. *Psychol. Methods* 1, 30–46.
- McNair, P.J., et al., 2002. Stiffness and passive peak force changes at the ankle joint: the effect of different joint angular velocities. *Clin. Biomech.* 17, 536–540.
- Nordez, A., et al., 2010. Improvements to Hoang et al.'s method for measuring passive length–tension properties of human gastrocnemius muscle in vivo. *J. Biomech.* 43, 379–382.
- Slapa, R.Z., et al., 2012. Shear wave elastography may add a new dimension to ultrasound evaluation of thyroid nodules: case series with comparative evaluation. *J. Thyroid. Res.* 2012, 657147.
- Ward, S.R., et al., 2009. Are current measurements of lower extremity muscle architecture accurate? *Clin. Orthop. Relat. Res.* 467, 1074–1082.
- Weiss, P.L., Kearney, R.E., Hunter, I.W., 1986. Position dependence of ankle joint dynamics – I. Passive mechanics. *J. Biomech.* 19, 727–735.
- Winters, T.M., et al., 2011. Whole muscle length–tension relationships are accurately modeled as scaled sarcomeres in rabbit hindlimb muscles. *J. Biomech.* 44, 109–115.
- Zajac, F.E., 1989. Muscle and tendon: properties, models, scaling, and application to biomechanics and motor control. *Crit. Rev. Biomed. Eng.* 17, 359–411.